

Geometric Alignment of Helical Tomographic Projection Data Using Pi-Lines

Andrew Kingston¹, Andreas Maniotis², Trond Varslot¹, Glenn Myers¹, Adrian Sheppard¹,
Jochen Trumpf², and Richard Hartley²

¹Department of Applied Math., Research School of Physics & Eng., CPMS, The Australian National University, Canberra 0200, Australia [email: andrew.kingston@anu.edu.au]

²Computer Vision and Robotics, CECS, The Australian National University, Canberra 0200, Australia [email: richard.hartley@anu.edu.au]

Keywords: tomography, calibration, alignment, pi-lines, sharpness

ABSTRACT

This paper considers the work by (Panetta et al 2008) and (Hartley et al 2010) on self-calibration of cone-beam CT systems in the context of helical scanning trajectories. Their technique is based on minimising the difference between opposing rays (pi-lines) and applies only to data on a horizontal line through the center of the detector for a circular scanning trajectory. Therefore it only uses a small portion of the total data and can't be used for all misalignments, e.g., detector tilt. For data from a helical scan this ray-difference applies to the upper and lower edges of the Tam-Danielsson window. The data therefore spans the detector both horizontally and vertically meaning this technique can be used for all misalignments. It also uses information from the entire sample making it a robust technique. Here we investigate the performance of this method on helical-CT data and investigate it as an enhancement to robustness of our currently used tomogram sharpness maximisation technique.

1. INTRODUCTION

Geometric alignment of micro- and nano- computed-tomography (CT) components is not a trivial exercise. The position of the X-ray source and rotation/translation stage are required to be known to a tolerance of less than the imaging resolution of the system. Even if a system is physically aligned after imaging some calibration phantom, component drift due to thermal expansion can change the alignment parameter values significantly. A software method for post-acquisition alignment or self-calibration is desirable. Our group has found such software methods (e.g., Kingston et al 2011) to be so useful that physical alignment is rarely necessary (if ever).

Since 2010 our group has moved to a helical scanning trajectory. This satisfies Tuy's data sufficiency condition (Tuy 1983) which enables exact reconstruction techniques (e.g., Katsevich 2002) and extremely high cone-angles, i.e., high X-ray flux. However, it has a translation and rotation stage, has 9 misalignment parameters, a minimum of redundancy in imaging. It is therefore highly sensitive to misalignment. The standard circular scanning trajectory by contrast does not satisfy Tuy's condition and requires an approximate reconstruction technique such as (Feldkamp et al 1984). It however has only a single rotation stage, a total of 7 misalignment parameters, and redundant 360 degree scanning. It copes well with misalignments and inconsistencies as they appear as a slight blurring.

Robust and precise software alignment of helical systems is therefore essential. To overcome non-uniform resolution problems due to finite detector sampling we use a double-helix scanning trajectory (Varslot et al 2012). This adds significant redundancy to the data that makes alignment by maximising tomogram sharpness work well (Kingston et al 2011). However, if the data from one helix fails, or for cases where dose must be minimised, it may be necessary to align projection data from a single-helix trajectory. Sometimes in this case there is insufficient information/redundancy for sharpness to work well. Here we show that a method that minimises the difference between opposing rays (known as pi-lines) is the perfect counterpart to sharpness.

The remainder of this extended abstract is organized as follows: The experimental geometry is outlined in section 2. Based on this geometry, pi-lines are defined in section 3. In section 4 we present methods to determine geometric alignment of tomographic projection data. The proposed method using pi-lines is outlined in section 4.1 followed by a brief review of the existing method used at our micro-CT facility: sharpness, in section 4.2. The performance of these measures, along with a hybrid, is investigated in section 5. Lastly, some concluding remarks are included in section 6.

2. EXPERIMENT GEOMETRY

Here we assume a lensless fine-focus geometry where magnification is achieved through the expanding spherical wave-front of X-rays emitted from a micro(nano)-focus X-ray source (S) that is a distance R from the rotation axis. A flat-panel detector (D) is located a distance L from the rotation axis (in the opposite direction; see Figure 1.). The object (or equivalently: source/detector) translates vertically by Z per revolution. Source position at angle θ is denoted S_θ , likewise detector position at angle θ is denoted D_θ . The coordinates on the detector are (w,h) , for w = width and h = height and $-N/2 \leq w,h < N/2$, with the origin at the center of the detector.

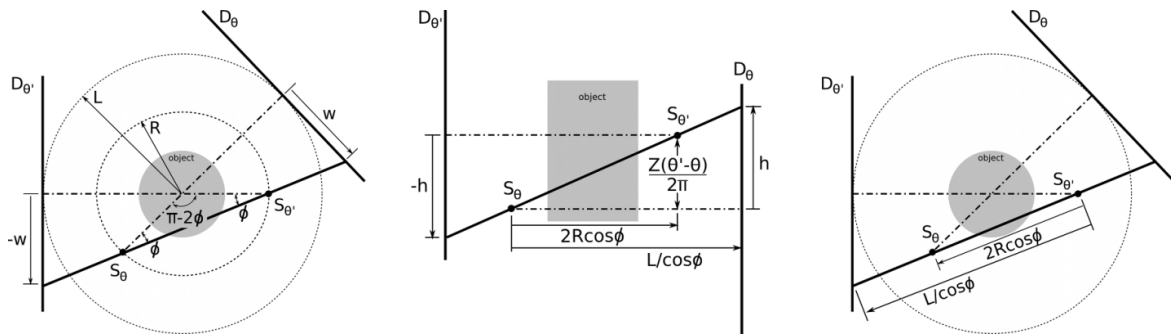


Figure 1: Depiction of experiment geometry and occurrence of equal but opposite ray paths (pi-lines).

3. PI-LINES

We are interested in finding the set of x-ray paths from S_θ to $D_\theta(w,h)$ denoted as ray $R_\theta(w,h)$ for which there exists another ray $D_{\theta'}(w',h')$ that has an equivalent direction but with the opposite trajectory. We can see from Figure 1 that $w' = -w$ and $h' = -h$ and defining $\phi = \arctan(w/L)$, then $\theta' = \theta + \pi - 2\phi$. Two ray paths that have opposing ray paths exists for each horizontal position, w ; They coincide with the upper and lower edges of the Tam-Danielsson window, h_u and h_d . It is sufficient to determine only one of these h values due to symmetries, i.e., $h_d(w) = -h_u(-w)$. Therefore it remains to determine h_u as follows:

$$h_u = Z(\pi - 2\phi) / (4\pi R \cos^2 \phi). \quad (1)$$

Tam-Danielsson (TD) window (Tam et al 1998, Danielsson et al 1997) defines a non-redundant (minimum) region of projection data required for reconstruction. Pi-lines first defined in (Danielsson et al 1997) define the boundaries of the window. If one were to draw the source trajectory in 3D space, the TD window is the projection of this trajectory onto the detector. One very important property of pi-lines is that each voxel in the tomogram belongs to a unique pi-line (Danielsson et al 1997, Defrise et al 2000). This implies that any method using pi-lines is probing the entire data set.

4. GEOMETRIC ALIGNMENT MEASURES

4.1. Pi-line difference

Suppose there exist M rays, $R_\theta^m(w, h_u)$ for $1 \leq m \leq M$, with opposing rays, $R_{\theta + \pi - 2\phi}^m(-w, -h_u)$. We then define the pi-line difference, Δ , as follows:

$$\Delta = \text{Sum}_m (R_{\theta}^m(w, h_u) - R_{\theta'}^m(-w, -h_u))^2 / M, \tag{2}$$

with h_u and θ' defined as above. The normalisation by M becomes important in implementation since the value of M can vary significantly for various misalignments.

One can determine Δ analytically for various misalignments; This is of course the fastest. We however already have code to align projection data onto virtual projections for each given misalignment parameter set. The process is therefore: for each misalignment parameter set given, remap the data to an aligned projection then compute Δ directly on these projections.

4.2. Sharpness

Sharpness is calculated as the L_2 norm of the reconstructed image gradient. For 3D reconstructions we select up to 9 2D slices distributed throughout the 3D reconstruction volume on which to calculate sharpness. If the selected slices are relatively featureless then sharpness may not perform well over some parameters. As can be seen in Figure 2 peaks in sharpness can be highly localised and difficult to find.

5. PERFORMANCE OF ALIGNMENT MEASURES

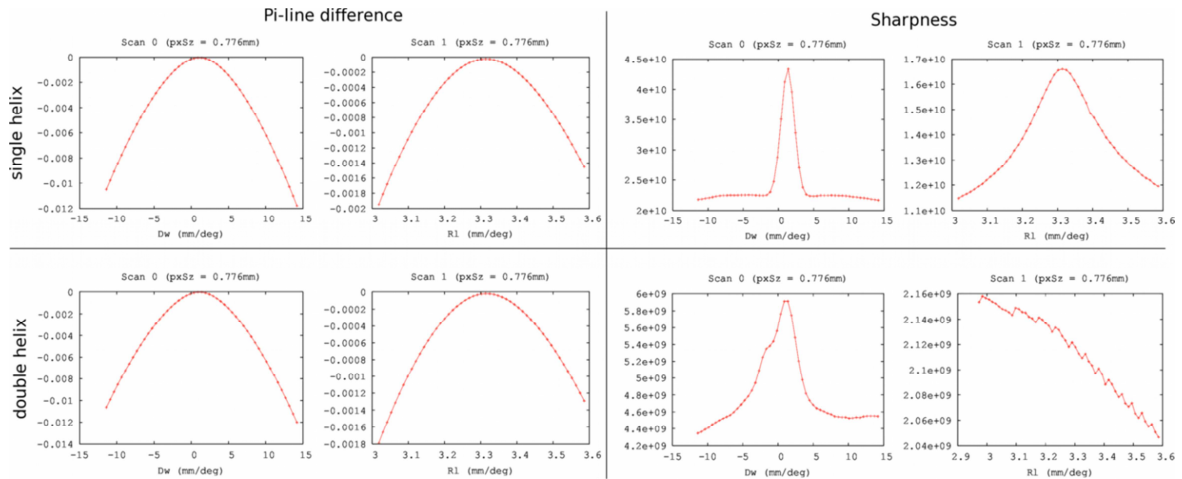


Figure 2: Search for detector shift (Scan 0: Dw) followed by R (Scan 1: RI) using both Pi-line-difference and Sharpness measures for both single- and double-helix trajectories.

The plots in Figure 2 show that pi-line difference has broader peaks (less precise) but is unchanged (more robust) when reduced from double- to single-helix data. Sharpness fails in single-helix Dw search (Scan 0) and therefore cannot locate a peak in RI search (Scan 1). Peaks in sharpness although more prominent due to high-frequency analysis but are consequently highly localised and easily missed. Peaks in pi-line difference are affected by high redundancy in low-frequency data and are thus much smoother.

Two new alignment techniques arise: 1) Multi-dimensional gradient based searches are likely to work quickly for pi-line difference to get close enough to the solution for sharpness to refine it, and 2) A hybrid alignment method: Sharpness/pi-line difference. This combines the low-frequency robustness of pi-line difference with the high-frequency precision of sharpness as has been demonstrated in Figure 3.

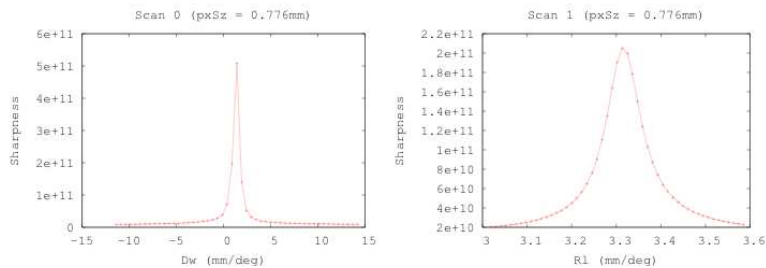


Figure 3: Search for detector shift (Scan 0: Dw) followed by R (Scan 1: Rl) using Hybrid:Sharpness/Pi-line-difference measures for both single-helix trajectory.

6. CONCLUSIONS

For helical scan projections, pi-line difference applies to data on the upper and lower edges of the Tam-Danielsson window spanning the detector both horizontally and vertically. This implies the technique can be used for all misalignments. It is affected by the redundancy of low-frequency data using information from the entire sample. This makes it a robust technique amenable to multi-dimensional gradient based optimisation techniques. However, it is not as precise as the high-frequency method based on sharpness. Pi-line difference can therefore act as a fast initial coarse alignment before refinement by sharpness, or can act as an enhancement to the robustness of tomogram sharpness maximisation technique as hybrid.

7. REFERENCES

- Danielsson, PE., Edholm, P., and Seger, M. (1997) Towards exact 3D-reconstruction for helical cone-beam scanning of long objects. A new detector arrangement and a new completeness condition Proc. 1997 Int. Meet. on Fully 3D Image Reconstruction in Radiology and Nuclear Medicine, pp 141-4.
- Defrise, M., Noo, F., and Kudo, H. (2000) A solution to the long-object problem in helical cone-beam tomography Phys. Med. Biol. 45 623-43.
- Feldkamp, L., Davis, L., and Kress, J. (1984) Practical cone-beam algorithm. J. Opt. Soc. Am., A(1):612-619.
- Hartley, R., Maniotis, A., Trumpf, J. (2010) Self-Calibration of a Cone-Beam CT Imager, Submitted to MICCAI.
- Katsevich, A. (2002) Theoretically Exact Filtered Backprojection-Type Inversion Algorithm for Spiral CT. SIAM Journal of Applied Mathematics 62(6): 2012-2026.
- Kingston, A., Sakellariou, A., Varslot, T., Myers, G., Sheppard, A. (2011) Reliable automatic alignment of tomographic projection data by passive auto-focus. Med Phys. 38(9):4934-45.
- Panetta, D., Belcari, N., Del Guerra, A., and Moehrs, S. (2008) An optimization-based method for geometrical calibration in cone-beam CT without dedicated phantoms. Phys. Med. Biol, 53(14):3841-3861.
- Tam, KC., Samarasekera, S., and Sauer, F. (1998) Exact cone-beam CT with a spiral scan Phys. Med. Biol. 43 1015-24.
- Tuy, H. (1983) An inversion formula for cone-beam reconstruction. SIAM Journal of Applied Mathematics, 43:546-552.
- Varslot, T., Kingston, A., Myers, G., and Sheppard, A. (2012) Considerations for high-magnification high-cone-angle helical micro-CT. Proc. SPIE 8506, Developments in X-Ray Tomography VIII, 8506-14.